Nonlinear scaling analysis of glucose metabolism in normal and cancer cells

V. Krishnan Ramanujan
Brian A. Herman
University of Texas Health Science Center at San Antonio
Department of Cellular and Structural Biology
7703 Floyd Curl Drive
San Antonio, Texas 78229

Abstract. Cancer progression is commonly accompanied by an altered glucose metabolism. In general, spatially resolved imaging of glucose metabolism and its subtle alterations might provide valuable diagnostic information *in vivo*. A classical example is positron emission tomography that exploits this feature in obtaining preferential accumulation of fluorescent analog of glucose in tumors, thereby achieving an imaging contrast. We report a novel scaling analysis of glucose metabolism in mammary epithelial (NMuMG) cells by detrended fluctuation analysis of Cerulean (cyan fluorescent protein variant) fluorescence. Fluorescence fluctuations of Cerulean are reasoned to be indicative of dynamic pH changes associated with glucose metabolism. Normal parental cells and the spontaneously transformed (cancerous) NMuMG cells displayed robust scaling exponent that reflects nonrandom fluctuations in Cerulean fluorescence. Acute dependence of cancer cells on glycolysis as compared with normal cells is exploited to yield a statistically significant difference in scaling exponent, thereby providing discrimination between normal and cancer cells *in vitro*. By careful design of experiments *in vivo*, the proposed scaling approach might even have diagnostic potential for early detection of cancer lesions in small animal models. [DOI: 10.1117/1.2928154]

Keywords: multiphoton processes; fluorescent protein; nonlinear dynamics; scaling; glucose metabolism; cancer; fluorescence lifetime imaging (FLIM).

Paper 07323SSR received Aug. 13, 2007; revised manuscript received Dec. 29, 2007; accepted for publication Dec. 31, 2007; published online May 22, 2008.

1 Introduction

A characteristic property of invasive cancers is altered glucose metabolism.[1] Biochemical assays for measuring this important metabolic activity have given useful kinetic information in a variety of cancers. However, the precise regulatory dynamics of glucose metabolism in intact living cells is far from clear. Studies have indicated that there are short-term and long-term changes in pH in various organelles (cytosol, mitochondria, lysosomes, etc.) during substrate metabolism and apoptosis.[2,3] Living cells tightly regulate pH homeostasis in normal conditions as well as under stress. One of the biochemical hallmarks of tumors is up-regulation of glycolysis even in the presence of oxygen (aerobic glycolysis or Warburg effect), thereby leading to increased lactic acid production as compared to normal, untransformed cells.[4] This led us to hypothesize that single-cell pH measurements during glucose metabolism may be valuable in assessing differences between normal and cancer cells.

In this paper, we have systematically characterized fluorescence intensity and lifetime kinetics of an improved version of cyan fluorescent protein[5] (Cerulean) in mammary epithelial cells during glucose metabolism. We recently reported adaptation of a nonlinear dynamical scaling analysis in a single-cell imaging paradigm where we observed that liver cells displayed complex dynamics and scaling behavior in redox fluctuations and free radical fluctuations.[6,7] Here, we extend this novel application for gaining insight into the regulatory nature of glucose metabolism in normal and transformed (cancerous) mammary epithelial cell lines. For this scaling analysis, we have exploited the fact that fluorescent proteins exhibit fluorescence fluctuations of the order of milliseconds in a pH-dependent as well as conformation-dependent manner.[8] Together, our data reveal complex dynamics in living cells manifested as regulatory time correlations in glucose metabolism. Initial theories for understanding glycolytic-flux control held the view that "rate-limiting enzymes" such as phosphofructokinase determine the entire metabolic flux; however, reevaluation by metabolic control analysis has confirmed that control is generally distributed, and effective physiological control of metabolic regulation can be shown to involve multiple sites simultaneously through action on a number of enzymes.[9] These recent observations point to a more complex network for glucose metabolism rather than an apparently "linear" array of enzymes. Our long-term goal is to understand experimental manifestations of such network complexity at the level of single cells.

Address all correspondence to V. Krishnan Ramanujan, PhD, Research Scientist I, Cedars-Sinai Medical Center, Minimally Invasive Surgical Technologies Institute (MISTI), Department of Surgery, 8700 Beverly Blvd., Los Angeles, CA 90048-3034; Tel: 310–423–7785; Fax: 310–423–7707; E-mail: ramanujanv@cshs.org

1083-3668/2008/13(3)/031219/7/$25.00 © 2008 SPIE

2 Materials and Methods

2.1 *Cell Culture*

The cells used in this study are the untransformed, parental mouse mammary epithelial cell line (NMuMG) and a spontaneously transformed, malignant cell line (NMuMG-ST) originally reported by Bandyopadhyay et al.[10] The NMuMG cell line was established through spontaneous immortalization of normal mouse mammary epithelial cells. The "normal" cells exhibit many untransformed features. The NMuMG-ST cells were isolated from these parental cell lines using a modified soft agarose assay. In this assay, sustained anchorage-independent growth potential of spontaneous transformed cells was exploited in successful isolation of a small number of transformed NMuMG-ST cells ("cancerous"). These transformed cells displayed focal, multilayer growth and higher saturation density in comparison with the normal, untransformed cells. Furthermore, these cells could also induce carcinomas when transplanted into nude mice with an ability to metastasize. Both the normal and ST cell lines were maintained in McCoy's 5A medium supplemented with 10% fetal bovine serum, pyruvate, vitamins, amino acids, and antibiotics. Working cultures were maintained at 37°C in a humidified atmosphere of 5% CO_2. For generating stable cells lines expressing Cerulean (a kind gift from Dr. David Piston, Vanderbilt University) construct, cells were transfected with cDNA of Cerulean construct using FuGene transfection kit (Roche, Indianapolis, Indiana). After the first day of transfection, the cells were maintained under selection pressure using Geneticin at 400 μg/ml concentration for 10 successive generations. The tenth generation stable cells were sorted using flow cytometry for high and medium expression clones. All the cells used in the present experiment are from the high Cerulean expression batch. A separate vial of frozen cells were thawed and subcultured before every experiment to avoid reversal of nontransformed features in NMuMG-ST cell lines.

2.2 *Fluorescence Intensity and Lifetime Imaging*

Imaging experiments were performed in a modified, homemade, two-photon fluorescence intensity imaging system (Olympus IX-71; Titanium; Sapphire femtosecond laser; 76-MHz repetition rate; 60×, 1.2 NA, water immersion; 25°C). Two-photon emission from Cerulean was maximal at 840-nm excitation, and the average power at the entrance of the scanning system was typically 10 to 15 mW. The actual power at the specimen was not measured. These excitation conditions were optimal for minimal or no photobleaching of Cerulean during kinetic experiments. Fluorescence emission was collected in a non-descanned detection configuration through a 480/40-nm emission filter (Chroma Technology Corp., Rockingham, Vermont). The fluorescence lifetime imaging (FLIM) system employed in this study was described in earlier publications.[11] Briefly, this system utilizes the same microscope and two-photon laser that are employed for intensity-imaging experiments. However, the laser emission, from the Ti:Sapphire laser is directed through a pulse picker and a custom-made FLIM optics so as to excite the specimen through the right port of the microscope. The fluorescence emission is directed to the streakscope (C4334, Hamamatsu Photonics, Japan: time-resolution ~50 ps) through a system of imaging lens and photocathode slit. The streakscope consists of a photocathode surface, a pair of sweep electrodes, a microchannel plate (MCP) to amplify photoelectrons coming off the photocathode, and a phosphor screen to detect this amplified output of MCP. Two beam scanner mirrors are employed for scanning along the x and y directions in the effective field of view ($\sim 40 \times 40$ μm). Synchronous x and$y$ scanning renders a stack of (x,y,t) streak images. This stack contains the complete information of optical intensity as well as the spatial and temporal information from the optical image. Numerical processing of all these streak images (i.e., the exponential decay profiles at every pixel of the raw streak image) gives the final FLIM image. In this way, complete information on fluorescence decays is obtained on a per-pixel basis.

2.3 *Time-Series Data Acquisition and Analysis*

Time-series data for monitoring Cerulean fluorescence fluctuations in living cells were acquired as follows: A field of view with ~4 to 6 cells was chosen before measurements. For achieving high time resolution, a line scan was performed so that the chosen line spanned all the cells. Typically, time-series data were acquired for $N=8000$ time points (~30 ms/line; ~58 μs/pixel). Every line scan samples the cell, yielding typically 100 to 300 individual time series depending on the region of interest. By averaging this set of time-series data, one. obtains a good statistical score of probing the spatiotemporal dynamics in single cells. In the present study, we are interested in asking how glucose metabolism in normal and cancer cells differs in different time scales (pixel time series: ~μs; lines scan time series: ~ms; and frame scan time series: ~s to min). Scaling analysis is an elegant way to probe real-time regulatory dynamics by analyzing subtle signal fluctuations (fluorescence fluctuations in the present case) that attempts to look for time correlations between the signal (or process) at any instant and the same signal (or process) at some other instant. If there are no apparent correlations between various time windows, then the underlying process can be assumed to be a "random" process. Brownian diffusion is a classical example of a random process (Brownian noise) with no apparent long-range time correlations. On the other hand, a nonrandom scaling behavior may indicate positive regulatory correlations that control the cellular process. Toward this end, we applied an analytical method, namely, detrended fluctuation analysis (DFA), originally developed by C.-K. Peng et al., to quantify statistical correlations in a time-series signal.[12,13] The DFA approach is a modified root-mean-square fluctuation analysis of Random walk—to quantify statistical correlations in a nonstationary time series signal. Figure 1 describes a schematic of this analysis procedure. The original time series (of length N) is first integrated and then divided into boxes of equal size (n). In each box, the integrated profile is fit to a polynomial that gives a local trend in that box. Next this local trend is subtracted from the integrated profile in each box, which is termed "detrending." Last, rms fluctuation $F(n)$ is calculated from the integrated and detrended signals in each box. These steps are repeated for different values of box size (n) to generate $F(n)$ for a broad range of scale sizes n. Intuitively, $F(n)$ will increase as n increases, and for scale-invariant signals

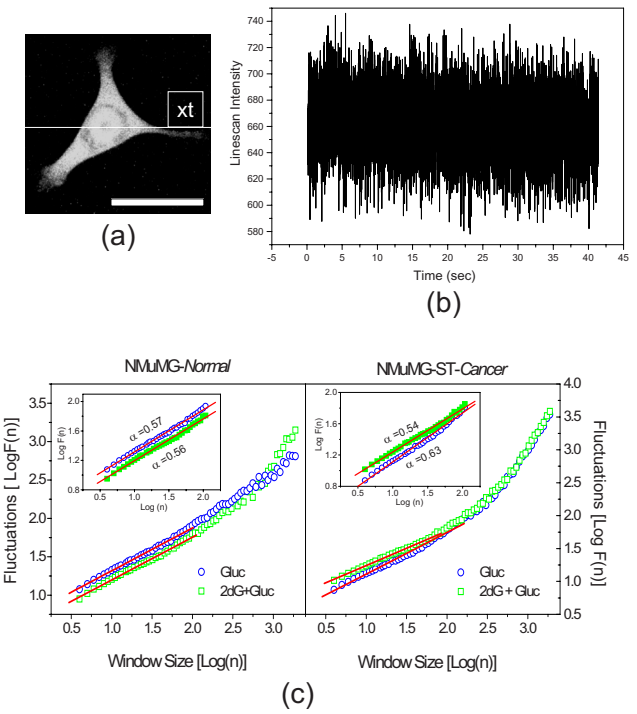

Fig. 1 Schematic of detrended fluctuation analysis (DFA) of line scan time series data. (a) Representative intensity image where line scan time series were obtained. The *xt* line spans typically 300 to 512 pixels, depending on the field of view, thereby rendering the same number of pixel time series; scale bar=20 μm. (b) Representative time series data acquired with 30 ms/line scan and $N=8000$ total line scans. This renders probing the dynamics in the time scales of a few hundred microseconds (pixel dwell time) to a few hundred milliseconds (line scan duration) and eventually to few seconds (entire time series data). We employed DFA in obtaining scaling function from the raw time series. More details about this method are described in the text. In brief, DFA dissects the original time series data into many windows with progressively increasing scale size (n) and calculates the rms fluctuations $F(n)$ for every scale size (n) to yield a scaling function $F(n)=n^{\alpha}$. The scaling exponent α is a quantitative measure of the extent of correlations in the signal. α can characterize randomness ($\alpha=0.5$ for white noise; $\alpha=1.5$ for Brownian noise) or correlations ($\alpha<0.5$ for anticorrelations, and $0.5<\alpha<1.5$ for persistent power law–like correlations), regardless of the nature or source of the fluctuations. (c) Representative scaling functions $F(n)=n^{\alpha}$ for normal and cancer cells with and without glycolytic inhibitor treatment. The inset shows an enlarged view of the fitted region ($0<\log n<2.0$) where the scaling exponent α was calculated.

with power-law correlations, there is a scaling relationship $F(n)=n^{\alpha}$. The scaling exponent α is a quantitative measure of the extent of correlations in the signal. α can characterize randomness ($\alpha=0.5$ for white noise; $\alpha=1.5$ for Brownian noise) or correlations ($\alpha<0.5$ for anticorrelations, and $0.5<\alpha<1.5$ for persistent power law–like correlations), regardless of the nature or source of the fluctuations. In other words, the scaling function is universal and can be used to analyze fluctuations in any time-series signal. Similar crossover in exponents has been noted in earlier studies of physiological signals. An important advantage of the DFA algorithm over other time-series analysis methods is that it can also be reliably used for nonstationary signals since local detrending eliminates the errors associated with nonstationary signals. Although this algorithm has been successfully used in quantifying correlations in physiological signals such as heartbeat dynamics and human gait dynamics, to the best of our knowledge, we were the first to carry out systematic application of this approach to understand single-cell dynamics in living cells. More details about this algorithm can be found in Ref. 6, and source code can be obtained from the webpage of the National Research source, at www.physionet.org.

2.4 *Statistics*

The data presented in this study are from at least three independent experiments. Statistical significance was determined by one-way ANOVA test where indicated.

3 Results

Although fluorescein-based ratiometric pH probes (e.g., BCECF) have a good dynamic range, we were interested in evaluating fluorescent protein-based pH probes, since these can be utilized in tumor models *in vivo*. Many fluorescent protein mutants have shown variable pH sensitivity, with maximum pH sensitivity being displayed by enhanced yellow fluorescent protein.[3] In this paper, we have systematically characterized pH dependence of an improved version of enhanced cyan fluorescent protein, namely, Cerulean, reported by Rizzo et al..[5] Normal and cancer phenotypes can be clearly distinguished by multilayer growth in the latter [Fig. 2(a)]. Figure 2(b) shows the pH calibration curve for Cerulean stably expressed in parental MMuMG cells. It is seen that Cerulean lifetime displayed a good dynamic range of pH sensitivity: $\Delta\tau=\pm 13\%$ ($\Delta\tau\sim 17\%$ at pH 5, and $\Delta\tau=13\%$ at pH 8) as compared to the lifetime at neutral pH. We carried out similar pH calibration experiments in cancerous NMuMG cells and obtained identical results (data not shown). This result is not surprising considering the fact that the pH calibration protocol required clamping of the buffer pH with nigericin. In order to test whether normal and cancer cells can show detectable differences in cytosolic pH during various perturbations that are known to alter cellular metabolism, we treated NMuMG and NMuMG-ST cells with mitochondrial complex inhibitors (rotenone and antimycin A) and apoptotic inducer staurosporine. As compared to control cells maintained at neutral pH 7, both normal and cancer cells show cytosolic acidification, as can been seen from the reduced lifetime of Cerulean [Fig. 2(c)]. Interestingly, cancer cells showed significantly larger acidification than the normal cells when mitochondrial electron transport was inhibited.

Although this result does not conclusively demonstrate that the observed decrease in cytosolic pH is directly due to the effect of mitochondrial inhibitors, it is highly probable that the observed differences between normal and cancer cells (in the presence of mitochondrial electron transport inhibitors) are indicative of alterations in mitochondrial response as well as in cytosolic pH. Some earlier studies have used oxygen depletion (either by growing cells in nitrogen atmosphere or by chemical hypoxia) for modulating cytosolic pH. We carefully avoided this approach to eliminate possible artifacts in cancer cell discrimination since hypoxia is known to have dissimilar effects on glucose metabolism in normal and cancer cells. Next, we wanted to see whether we could monitor real-time lifetime modifications while the cells are metabolizing

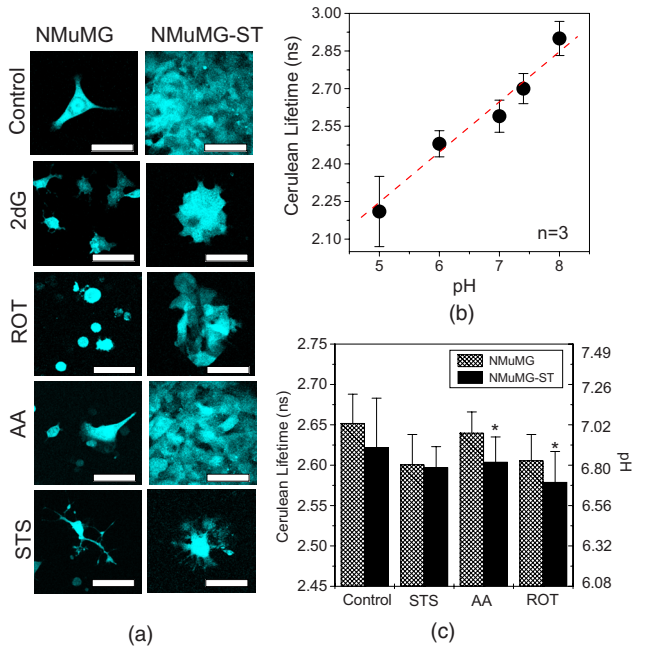

Fig. 2 Steady-state lifetime imaging in normal and cancer cells during metabolic perturbations. NMuMG and NMuMG-ST cells stably expressing Cerulean in cytosol were imaged in a custom-made two-photon imaging system, (a) Representative intensity images of cells either untreated (control) or treated with mitochondrial complex I inhibitor (10 μM rotenone; 4 h; 37°C), complex III inhibitor (10 μM Antimycin A; 4 h; 37°C), apoptosis inducer (1 μM staurosporine; 4 h; 37°C), or glycolytic inhibitor (20 mM 2-deoxyglucose; 4 h; 37°C); scale bar=20 μm. (b) pH calibration curve showing fluorescence lifetime versus pH for Cerulean. The cells were maintained in high K^+ buffers at varying pH 5, 6, 7, and 8 at 37°C for 30 min before imaging at room temperature. All the experiments at fixed pH were performed by clamping pH with 5 μM nigericin in the pH buffers. (c) Steady-state lifetime histograms (with corresponding pH scale shown in the right y axis, as calculated from the pH calibration curve) of normal and cancer cells under representative metabolic perturbations. Data are shown as mean±SEM, pooled from 3 to 5 experiments. Statistical significance in (c) was obtained from a one-way ANOVA test with $p<0.05$.

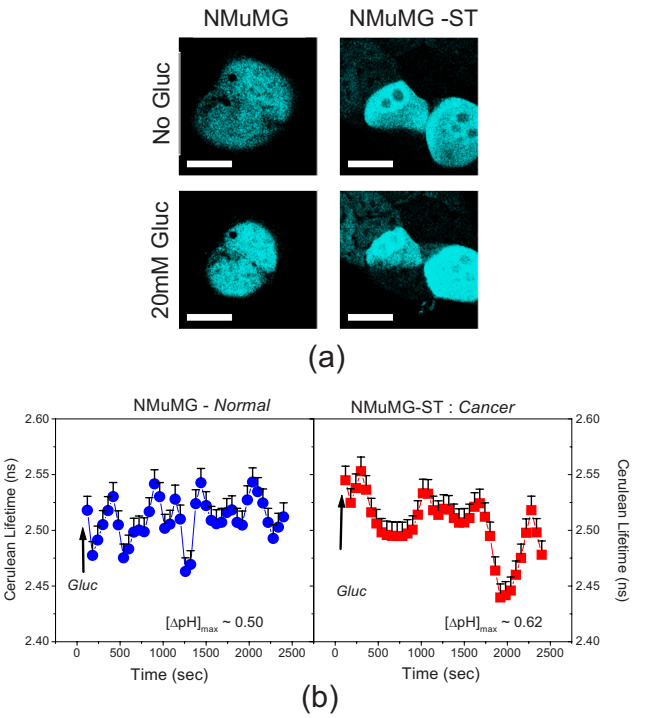

Fig. 3 Glucose-induced lifetime changes in NMuMG and NMuMG-ST cells. (a) Representative 2p-fluorescence images of normal and cancer cells expressing Cerulean pre- and post-glucose stimulus. 20 mM glucose was added during kinetic experiments, and images were collected subsequently to analyze the glucose-induced fluorescence decay curves; scale bar=20 μm. (b) Representative lifetime kinetic profiles in NMuMG and NMuMG-ST cells with a single 20 mM glucose pulse as indicated by an arrow. All experiments were performed at room temperature (25°C). Typically, 20 to 30 cells were imaged per experiment, and the displayed results are representative of $n=4$ experiments in the case of pH kinetics and $n=6$ experiments in the case of scaling measurements. A typical data acquisition time was ~3 min per line scan per imaging chamber ($n=4$ cells; scaling measurements) and ~20 min per imaging chamber ($n=6$ cells; pH kinetics).

glucose. A single pulse of glucose transiently decreases Cerulean lifetime, but continuous monitoring of Cerulean lifetime after the glucose pulse showed that normal and cancer cells differ in the recovery of homeostasis (Fig. 3). Normal cells displayed an oscillatory lifetime profile indicative of approach to restore the pH equilibrium. However, the cancer cells displayed two larger reductions in Cerulean lifetime, clearly suggesting that normal and cancer cells are significantly different in their ability to metabolize glucose at the single-cell level. Even though we have not demonstrated a direct connection between glucose metabolism and pH changes, the only reasonable explanation of this observation can be attributed to hyperactivity of glucose metabolic machinery (either increased glucose transporters or increased glycolytic rate or both) in cancer cells.

We next addressed the issue of regulatory dynamics of intracellular glucose metabolic machinery. We recently reported long-range time correlations in fluorescence fluctuations characteristic of subcellular regulatory dynamics.[6] By analyzing scaling parameters in time-series data from intact living cells, we observed that mitochondrial redox fluctuations and free radical signal fluctuations displayed nonrandom correlations.[6,7] Figures 1(a) and 1(b) demonstrate the schematic of the scaling analysis procedure in intact living cells, and the figure caption describes the premise of the scaling analysis procedure. Earlier studies, including our recent reports, have pointed out that regulatory correlations may decrease during aging and in diseases.[14,15]

With this rationale, we wanted to test whether scaling analysis of Cerulean fluorescence fluctuations can yield additional information on the regulatory nature of glucose metabolism in normal and cancer cells. We acquired an extensive set of time-series data from living cells (normal and cancer) where we monitored Cerulean fluorescence fluctuations before and during glucose stimulus. Figure 1(c) shows representative scaling functions $F(n)=n^{\alpha}$ calculated from the Cerulean time series in NMuMG and NMuMG-ST cells. The insets show a magnified view of the fitted regions where the scaling exponent α was determined. Since cancer cells are expected to show more sensitive dependence on glycolysis than the normal cells, we also obtained scaling exponents un-

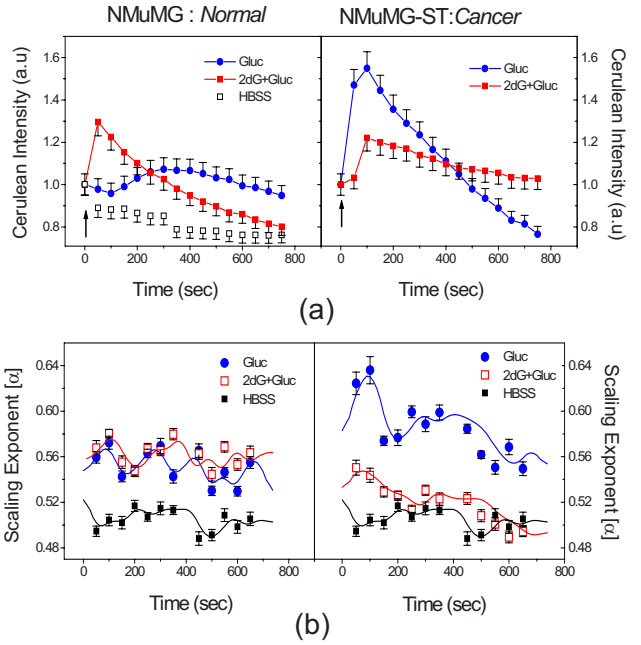

Fig. 4 Glucose-induced modifications in scaling exponent. (a) Two-photon fluorescence intensity kinetic profiles in normal and cancer cells with and without glycolytic inhibitor, 2-deoxyglucose (2dG). A single glucose pulse (20 mM) transiently increases Cerulean intensity, probably due to the cytosolic pH buffering, and the decay curves display dramatic difference between normal and cancer cells. In line with these intensity kinetics, the kinetic profiles of scaling exponents (b) reveal that normal cells are robust under glycolytic inhibition treatment (control: α=0.55; 2dG: α=0.55), whereas cancer cells completely lose regulatory correlations (control: α=0.63; 2dG: α=0.53), indicating that cancer cells acutely depend on glycolysis more than the normal cells.

der the conditions of glycolytic inhibition (2-deoxyglucose). As can be seen from these figures, the normal cells are more robust in maintaining regulatory time correlations than cancer cells. In the latter, glycolytic inhibition almost completely suppresses the nonrandom scaling behavior, thereby reducing the scaling exponent α from 0.63 to 0.54.

It is worth mentioning here that this difference is highly significant since the exponent appears as the power of window size as in the scaling relationship: $F(n)=n^{\alpha}$. Fluorescence intensity measurements of Cerulean, although are not indicative of pH status in living cells, can provide useful kinetic information. Figure 4(a) shows kinetic profiles of Cerulean fluorescence emission in normal and cancer cells when stimulated by a single glucose pulse. As can be seen from the kinetic profiles, normal and cancer cells differ in their instantaneous fluorescence decay rates. Normal cells have a faster decay rate probably due to an innate adaptive response to glycolytic inhibition. However, the cancer cells show a dramatic difference in glucose metabolism rate after glycolytic inhibition, indicating that glycolytic dependence is still preserved in these cells. Figure 4(b) shows a time course of scaling exponent α during glucose metabolism in normal and cancer cells. Prior to glycolytic inhibition, it can be seen that both normal and cancer cells displayed nonrandom ($\alpha>0.5$) correlations in Cerulean fluorescence fluctuations, indicating that-there is a regulatory network operative in these epithelial cells. Since the primary goal of this paper is to test whether single cells exhibit regulatory network correlations rather than identifying the individual members of the network, we would like to treat the observed scaling response in normal and cancer cells as a global response of the entire glucose processing machinery. With this in mind, it is intriguing to note that cancer cells have a significantly higher value of scaling exponent during glucose metabolism. This will be further discussed in the next section. In line with the kinetic profiles, we carried out scaling analysis in normal and cancer cells under glycolytic inhibition conditions as well. Figure 4(b) shows that normal cells indeed maintain the regulatory correlations even after preconditioning with glycolytic inhibitor, whereas the cancer cells show a significant reduction in scaling exponent upon 2dG treatment. In fact, the kinetic profile of scaling exponent after 2dG treatment looks similar to that when the cells were stimulated with Hanks' balanced salt solution (HBSS) buffer as a negative control.

4 Discussion

In this paper, we have carefully exploited the fluctuation regime dynamics of fluorescent protein Cerulean and explored a novel possibility for applying the scaling analysis as a tool in understanding the regulatory nature of glucose metabolism in living cells. Cerulean is a recent addition to the gamut of fluorescent protein variants. For the first time, we have systematically explored the pH dependence of this protein in living cells. Cerulean lifetime displayed a robust pH-sensitive response of $\Delta\tau=\pm 13\%$ above and below neutral pH. Metabolic perturbations such as staurosporine (protein kinase inhibitor and apoptosis inducer) and mitochondrial complex inhibitors (that will alter glycolytic rates) consistently showed cytosolic acidification [Fig. 2(c)]. Cancer cells displayed significantly higher acidification owing to the fact that they usually display more glycolytic dependence. Our data are in agreement with earlier reports where these treatments are known to acidify cytosol and/or mitochondria.[3] Further, glucose stimulus transiently increased the fluorescence emission of Cerulean (time scale ~60 s), possibly due to the transient buffering capacity of acidified cytosol. Kinetic measurements of fluorescence lifetime revealed an interesting discrimination between normal and cancer cells (Fig. 3). While normal cells have a tight oscillatory lifetime curve after the glucose stimulus indicative of pH homeostasis, the cancer cells are less efficient in restoring pH balance after glucose stimulus, as displayed by large reductions in Cerulean lifetime. Earlier reports have pointed out that cancer cells have increased expression of glucose transporter proteins (GLUTs). Since we did not measure the levels of GLUTs in normal and cancer cells, we cannot rule out the possibility that the difference in acidification can arise due to the difference in GLUT activity in cancer cells.

Thus, in step with the literature, it is possible that NMuMG-ST cells have an upregulated glycolytic pathway, thereby making these cells distinct from the normal cell phenotype. This assumption was further confirmed by the scaling analysis of fluorescence fluctuations in these cells, which revealed interesting features. First, the effect of glycolytic inhibition is less severe on normal cells, probably due to the fact that both mitochondrial and glycolytic machinery operate in

concert in these cells. On the other hand, glycolytic up-regulation in cancer cells seems to be not merely a sufficient condition for increased energy consumption but a necessary condition for cell proliferation and survival as displayed by the acute dependence on glycolysis. Second, scaling exponents offer a more reproducible way of distinguishing normal and cancer cells rather than fluorescence intensity alone since the latter can be affected by concentration and spectral artifacts. We have observed that scaling exponents are not affected by differences in absolute fluorescence intensity but are dependent only on the fluctuation dynamics (data not shown). This implies that scaling analysis might be a rapid diagnostic measure of altered glucose metabolism in *in vivo* tumors. It is to be noted that all our experiments were performed at 25 °C. Although the temperature per se does not affect the glucose metabolism kinetics (the intensity kinetic profiles as shown in Fig. 1(a) were identical at 25° and 37 °C) in our *in vitro* experiments, we cannot completely discard the possibility that these *in vitro* results may not be identical to real physiological metabolic status *in vivo*. Since we have not undertaken any *in vivo* experiments, it is difficult for us to predict the extent of differences. However, we can certainly speculate that if there are differences between our *in vitro* and future *in vivo* experiments, they may arise from other sources of physiological complexity in the animal models rather than just temperature dependence of pH and/or the scaling exponents.

There are two aspects to the observed scaling behavior that need attention: first, the photophysical nature of fluorescent protein (Cerulean) fluctuations, and second, the biological mechanism that gives rise to scaling phenomenon during glucose metabolism in living cells. Fluorescence correlation spectroscopic studies have revealed that the initial excited state process in green fluorescent protein (GFP) involves a proton transfer reaction and that fluorescence blinking of anionic GFP mutants is known to take place on a time scale of 45 to 300 ms, depending on pH.[16] A more recent time-resolved fluorescence/anisotropy study reported the structural basis of fluorescence fluctuation dynamics of GFPs in acidic environments.[8] These authors provided experimental evidence that the total fluorescence of the excited neutral state of GFP displayed a strong correlation between the fluorescence lifetime, structural conformation, and pH. Biexponential anisotropy decay analysis further suggested a segmental mobility of the chromophore associated with conformational changes of the protein, and this segmental motion became faster with an enhanced amplitude as the pH is reduced.

Thus, fluorescence fluctuations of GFP mutants including Cerulean as in this work can be rationalized by a subtle interplay of intracellular, pH dynamics and excited state dynamics of the fluorophore itself. More recent x-ray studies of Cerulean have revealed intriguing features such as shift in absorbance band in acidic pH (7 to 5) without significant modulation of fluorescence emission.[17] It was further suggested that acidification may be accompanied by a slow chromophore ionization from trans to cis form, and we speculate that Cerulean fluorescence fluctuations reported in this paper arise predominantly from excited state dynamics rather than conformational changes since these authors did not find evidence for multiple conformations of the protein.[17] As far as the biological mechanism behind the glucose-induced scaling behavior in normal and cancer cells, the observations are consistent with a tight regulatory network that encompasses glycolytic and mitochondrial OxPhos pathways. In this paper, we have attempted to correlate transient pH changes (as measured through lifetime imaging) and scaling behavior in intensity fluctuations (as measured through fluorescence intensity imaging). Although we have demonstrated a clear correlation between these two independent assays in discriminating normal from cancer cells, it will be certainly intriguing and worthwhile to directly probe scaling behavior in fluorescence lifetime fluctuations. The major impediment lies in the vast difference in data acquisition time in intensity and lifetime imaging approaches. For statistical robustness, it is imperative to sample many pixels (i.e, line scan) and to collect at least 6000 to 8000 time points. This condition implies that a line-scan time series ($N \sim 8000$ time points) could be obtained in ~ 200 s in the intensity imaging approach. On the other hand, the current lifetime imaging platform in our laboratory would require typically 40 min to obtain a line-scan time series. This prolonged data acquisition would defeat the purpose of monitoring fast, transient phenomena in the biological system under question. Furthermore, it is highly probable that the scaling exponents from such lifetime fluctuation measurements may not reflect the "true" nonlinear dynamical features but only some averaged, macroscopic behavior of the system.

In summary, we have reported a hitherto unknown scaling behavior in normal and cancer cells during glucose metabolism. To the best of our knowledge, this is the first demonstration of nonlinear dynamics in the glucose metabolizing network in living cells. Understanding tumor metabolism is the first step in designing efficient therapeutic intervention. Since tumors have higher probability for glycolytic up-regulation, targeting this evolutionarily conserved pathway can be a realistic approach for early detection of tumors *in vivo* as well as for targeting drugs for therapy. Since clinical modalities such as positron emission tomography (PET) already utilize preferential glucose uptake by tumors as a means to achieve imaging contrast, the scaling analysis reported in this paper might serve as a complementary tool in augmenting diagnostic information *in vivo*. Although we have no sufficient data to prove that scaling analysis is effective *in vivo*, we speculate that the present study is the first step in achieving that goal.

Acknowledgments

We thank Lu-Zhe Sun and Abhik Bandyopadhyay for their generous gift of NMuMG and NMuMG-ST cell lines. We gratefully acknowledge Gabriela Cantu for her initial help in pH measurements.

References

1. R. A. Gatenby and R. J. Gillies, "Why do cancers have high aerobic glycolysis?" *Nat. Rev. Cancer* **4**, 891–899 (2004).
2. J. Llopis, J. M. McCaffery, A. Miyawaki, M. G. Farquhar, and R. Tsien, "Measurement of cytosolic, mitochondrial, and Golgi pH in single living cells with green fluorescent proteins," *Proc. Natl. Acad. Sci. U.S.A.* **95**, 6803–6808 (1998).
3. S. Matsuyama, J. Llopis, Q. L. Deveraux, R. Y. Tsien, and J. C. Reed, "Changes in intramitochondrial and cytosolic pH: early events that modulate caspase activation during apoptosis," *Nat. Cell Biol.* **2**, 318–325 (2000).
4. J. W. Kim and C. V. Dang, "Cancer's molecular sweet tooth and the Warburg effect," *Cancer Res.* **66**, 8927–8930 (2006).
5. M. A. Rizzo, G. H. Springer, B. Granada, and D. W. Priston, "An improved cyan fluorescent protein variant useful for FRET," *Nat.*

Biotechnol. **22**, 445–449 (2004).
6. V. K. Ramanujan, G. Biener, and B. A. Herman, "Scaling behavior in mitochondrial redox fluctuation," *Biophys. J.* **90**, L70–72 (2006).
7. V. K. Ramanujan and B. A. Herman, "Aging process modulates nonlinear dynamics in liver cell metabolism," *J. Biol. Chem.* **282**, 19217–19226 (2007).
8. Y. Liu, H. R. Kim, and A. A. Heikal, "Structural basis of fluorescence fluctuation dynamics of green fluorescent proteins in acidic environments," *J. Phys. Chem. B* **110**, 24138–24146 (2006).
9. D. A. Fell and S. Thomas, "Physiological control of metabolic flux: the requirement for multisite modulation," *Biochem. J.* **311**(Pt 1), 35–39 (1995).
10. A. Bandyopadhyay, M. L. Cibull, and L. Z. Sun, "Isolation and characterization of a spontaneously transformed malignant mouse mammary epithelial cell line in culture," *Carcinogenesis* **19**, 1907–1911 (1998).
11. V. K. Ramanujan, J. H. Zhang, E. Biener, and B. Herman, "Multiphoton fluorescence lifetime contrast in deep tissue imaging: prospects in redox imaging and disease diagnosis," *J. Biomed. Opt.* **10**, 051407 (2005).
12. C. K. Peng, S. Havlin, H. E. Stanley, and A. L. Goldberger, "Quantification of scaling exponents and crossover phenomena in nonstationary heartbeat time series," *Chaos* **5**, 82–87 (1995).
13. C. K. Peng, S. V. Buldyrev, A. L. Goldberger, S. Havlin, F. Sciortino, M. Simons, and H. E. Stanley, "Long-range correlations in nucleotide sequences," *Nature (London)* **356**, 168–170 (1992).
14. H. E. Stanley, S. V. Buldyrev, A. L. Goldberger, Z. D. Goldberger, S. Havlin, R. N. Mantegna, S. M. Ossadnik, C. K. Peng, and M. Simons, "Statistical mechanics in biology: how ubiquitous are long-range correlations?" *Physica A* **205**, 214–253 (1994).
15. A. L. Goldberger, L. A. Amaral, J. M. Hausdorff, P. Ch. Ivanov, C. K. Peng, and H. E. Stanley, "Fractal dynamics in physiology: alterations with disease and aging," *Proc. Natl. Acad. Sci. U.S.A.* **99**(Supp 1), 2466–2472 (2002).
16. M. Chattoraj, B. A. King, G. U. Bublitz, and S. G. Boxer, "Ultra-fast excited state dynamics in green fluorescent protein: multiple states and proton transfer," *Proc. Natl. Acad. Sci. U.S.A.* **93**, 8362–8367 (1996).
17. G. D. Malo, L. J. Pouwels, M. Wang, A. Weichsel, W. R. Montfort, M. A. Rizzo, D. W. Piston, and R. M. Wachter, "X-ray structure of Cerulean GFP: a tryptophan-based chromophore useful for fluorescence lifetime imaging," *Biochemistry* (2007).